High-pressure structural changes in the $Gd_2Zr_2O_7$ pyrochlore

F. X. Zhang,[1] J. Lian,[1] U. Becker,[1] R. C. Ewing,[1,*] Jingzhu Hu,[2] and S. K. Saxena[3]
[1]*Department of Geological Sciences, University of Michigan, Ann Arbor, Michigan 48109, USA*
[2]*X17C, National Synchrotron Light Source, Brookhaven National Laboratory, Upton, New York 11973, USA*
[3]*The Center for Study of Matter at Extreme Conditions, Florida International University, Miami, Florida 33199, USA*
(Received 17 April 2007; revised manuscript received 28 September 2007; published 10 December 2007)

Pressure-induced structural changes in $Gd_2Zr_2O_7$ pyrochlore have been investigated at pressures up to 43 GPa by synchrotron x-ray diffraction and Raman scattering measurements. With increasing pressure, the ordered pyrochlore begins to transform to a disordered defect-fluorite-type (cubic) structure up to 15 GPa. Above 15 GPa, a high-pressure (HP) phase forms that has a distorted defect-fluorite-structure of lower symmetry. Upon release of pressure, the HP phase is not stable and gradually transforms back to the cubic defect-fluorite structure.

DOI: 10.1103/PhysRevB.76.214104 PACS number(s): 61.50.Ks, 61.10.Nz, 72.80.Ga

I. INTRODUCTION

The pyrochlore oxides, $A_2B_2O_7$, can be described as an ordered superlattice of the simple, isometric fluorite structure type, AX_2.[1,2] In the pyrochlore structure type, the *A*- and *B*-site (16*c* and 16*d*) cations alternate on the fcc sublattice in rows along the ⟨110⟩ directions. The anion sublattice is comprised of three different oxygen sites, two of which are occupied (8*a* and 48*f*), and the third site (8*b*) is vacant. Hence, the anion vacancies are ordered. The *A*-site cations are in eightfold coordination, and the *B*-site cations are in sixfold coordination. All anion sites are tetrahedrally coordinated: the 8*a* site is surrounded by four *A*-site cations. The 48*f* site (O2) is surrounded by two *A*- and two *B*-site cations that are slightly displaced from the center of the tetrahedral site toward the unoccupied 8*b* site. The magnitude of the displacement is represented by the positional parameter *x* of oxygen at the 48*f* site, which is 0.375 for the ideal fluorite structure. The tetrahedral site (8*b*) formed by four *B*-site cations is vacant. The anion vacancies in pyrochlore $A_2B_2O_7$ are arranged around the smaller *B*-site cations at distances $\frac{1}{2}\langle 111\rangle_{\text{fluorite}}$ and form a tetrahedral network. The structural transition from the pyrochlore (*P*-type) to the defect-fluorite (*F*-type) is an order-disorder transition, which requires disordering between *A*- and *B*-site cations, as well as disordering of the anion vacancies. During the order-disorder phase transition, changes in symmetry, lattice parameters, and coordination number of cations are observed.[1–6]

Pyrochlore oxides are one of the most promising candidate materials as ionic and electronic conductors.[1,7–9] Their structure and electronic properties depend on the disordering of cations and anions. The stability of the disordered structure is generally related to the ratio of ionic radii of the cations in the *A* and *B* sites.[1] Cation disordering greatly enhances the formation of anion Frenkel defects.[10–12] At normal pressure, the ordered pyrochlore structure can form for $r_A/r_B=1.46$ to 1.78 (Refs. 1, 6, and 13) and high-pressure or high-temperature synthesis can greatly extend this stability range.[14,15] Usually, smaller values of r_A/r_B favor the formation of disordered *F*-type structure.[11] The order-disorder transition from the pyrochlore to defect fluorite structure type may be induced by adjusting the composition,[1] increasing the temperature,[3] or by applying high-energy irradiations.[16] The disordering of cation and anion sublattices can occur independently.[17] Neutron scattering results in $Y_2(Ti_{1-x}Zr_x)_2O_7$ reveal that the anion disordering precedes cation disordering,[18] a result which is confirmed by *in situ* TEM observations.[19]

The *P*-type $Gd_2Zr_2O_7$, which has the smallest value of $r_{Gd3+}/r_{Zr4+}=1.46$, is one of the most interesting pyrochlores with $A_2B_2O_7$ stoichiometry and because oxygen conductivity increases with the degree of lattice disorder.[20] Its structure and degree of order in the binary system can be tuned by changing the stoichiometry and temperature. According to the phase diagram,[3] ordered pyrochlore can be formed in a ZrO_2-Gd_2O_3 system with a Gd content of 32–62 wt % at temperatures below 1500 °C. The *P*-type to *F*-type phase transition temperature for $Gd_2Zr_2O_7$ is about 1550 °C.[3] Recently, it was found that $Gd_2Zr_2O_7$ and other pyrochlore oxides are radiation-resistant ceramics that disorder to a defect-fluorite structure that does not become amorphous.[10,16,21–27] Sickafus *et al.*[11] have proposed that oxygen-deficient *F*-type $A_2B_2O_7$ structure with a random arrangement of the cations should be more stable upon irradiation. The lower the cation antisite defect energy (such as for $Gd_2Zr_2O_7$), the more readily will the radiation-induced transition to the disordered fluorite structure occur, thus leading to a material that does not amorphize. This has been demonstrated by irradiations with 2 MeV Au^{2+} and 1 MeV Kr^+ of $Gd_2Zr_2O_7$ that transforms the *P*-type to *F*-type structure at room temperature,[27] but unlike other pyrochlore oxides, this zirconate pyrochlore cannot be amorphized even at doses as high as ~100 displacements per atom (dpa).

Heavy ion irradiation of pyrochlore oxides leads to the distortion of the unit cell and the order-disorder transition occurs during the relaxation and recovery phase of the damage cascade. At high pressures, the unit cell is compressed and the order-disorder transition and even amorphization have been observed in Ti-based pyrochlore oxides.[28,29] The mechanism of pressure-induced phase transition in pyrochlore is not yet clear. In this paper, we describe the structural transitions of $Gd_2Zr_2O_7$ up to pressures of 43 GPa as monitored *in situ* by XRD and Raman measurements.

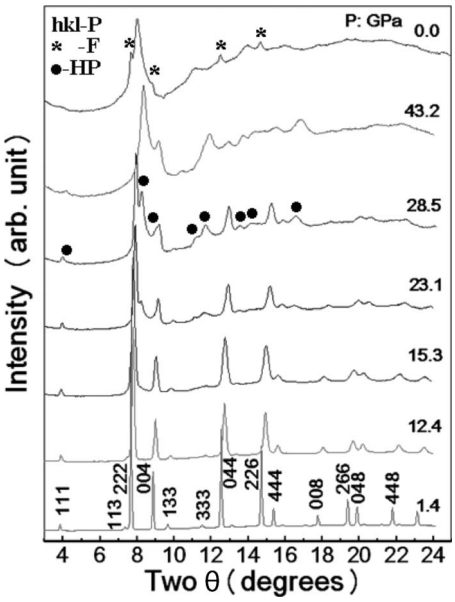

FIG. 1. XRD patterns of $Gd_2Zr_2O_7$ with increasing pressure. The pyrochlore structure is stable up to 15 GPa and transforms to a distorted fluorite structure at higher pressures. Some defect-fluorite structure is recovered from the sample after the release of pressure. A small amount of amorphous material is evidenced in the XRD patterns at high pressures. The diffraction peaks from the pyrochlore structure, high-pressure phase and the defect-fluorite structure are marked with Miller indexes, solid circles, and stars, respectively.

II. EXPERIMENT

A powder of $Gd_2Zr_2O_7$ pyrochlore was prepared by a sol-gel method with an aqueous mixture of zirconyl chloride solution and the appropriate rare-earth nitrate followed by a subsequent high-temperature treatment. The details of synthesis procedure are given elsewhere.[27] High-pressure experiments were performed in a diamond anvil cell with stainless steel gaskets. The angle dispersive x-ray-diffraction (XRD) experiments were performed at the X17C station at National Synchrotron Light Source, Brookhaven National Laboratory, with a monochromatic wavelength of 0.4066 Å. Raman spectra were collected by using a high-throughput holographic imaging spectrograph with a volume transmission grating, holographic notch filter, and a thermoelectrically cooled charge-coupled device system (physics spectra). The light source was a 783.54 nm He-Ne laser, and the laser power was controlled to be below 5 mW. Pressure in all of the experiments was calibrated by the standard ruby fluorescence method.[30] In order to compare the nonhydrostatic pressure effects of the phase transition, different pressure transmitting media, such as methonal/ethonal (4/1), argon, and nitrogen were used.

III. RESULTS AND DISCUSSION

Selected XRD patterns of $Gd_2Zr_2O_7$ up to 43.2 GPa are shown in Fig. 1. From ambient pressure up to 15.3 GPa, the pattern is that of a typical pyrochlore structure type. Above

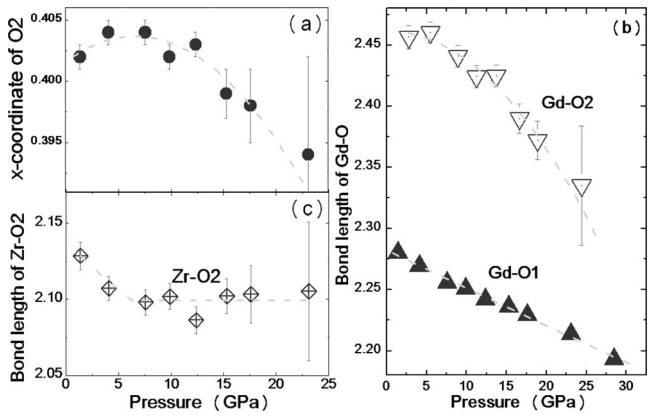

FIG. 2. (a) x coordinate of O2 at the 48f position, and (b) and (c) the cation-anion bond lengths in pyrochlore $Gd_2Zr_2O_7$ at various pressures. The data is derived from Rietveld refinement of the XRD patterns. The dashed line is a guide to the eyes and the error bar is marked on the data point. The large deviation at 23.2 GPa is due to the formation of the HP phase. The data of ⟨Gd-O1⟩ distance at 28.5 GPa is calculated from the indexed lattice constant.

15.3 GPa, a new high-pressure (HP) phase appeared, and this HP phase coexists with the pyrochlore structure up to 32.3 GPa. At higher pressures, only the pattern of pure HP phase is evident and remains up to 43.2 GPa. During the unloading process, the HP phase is stable at pressures greater than 3.5 GPa. In the quenched sample, some sharp peaks corresponding to the diffraction peaks of the F-type structure are evident, in addition to the diffraction peaks of the HP phase.

In the ordered pyrochlore structure, all of the atoms are on special positions, except the 48f oxygen. Hence, the structure is entirely described by the x positional parameter of the O_{48f}. The x-ray-diffraction patterns were refined by the Rietveld method up to 23.2 GPa. The refined x parameter for O_{48f} as a function of pressure is shown in Fig. 2(a). Below 10 GPa, there is no or little change, followed by a rapid decrease with increasing pressure. At ambient pressure $x=0.402$, but it decreases to 0.394 at 23.2 GPa, thus approaching the ideal F-type structure ($x=0.375$). The corresponding change of ⟨Gd-O⟩ bond length is shown in Fig. 2(b). The bond length of ⟨Gd-O1⟩ changes nearly linearly with the decrease in the lattice constant. At pressures greater than 10 GPa, the ⟨Gd-O2⟩ bond length decreases more rapidly than that of ⟨Gd-O1⟩. The ⟨Zr-O2⟩ bond length in the ZrO_6 octahedra is also shown in Fig. 2(c). The ⟨Zr-O2⟩ bond length decreases with pressure up to 5 GPa. Above that pressure, there is little change. As a result, the ratio of bond length between cations and anions changes from 1.07 at 1 atm pressure to 1.05 at 23.2 GPa for $d_{\text{Gd-O1}}/d_{\text{Zr-O2}}$ and from 1.15 to 1.10 for $d_{\text{Gd-O2}}/d_{\text{Zr-O2}}$. The x coordinate in the ideal fluorite is 0.375 and $r_{A\text{-O}}/r_{B\text{-O}}=1$. Thus, the $Gd_2Zr_2O_7$ pyrochlore has a tendency to change from the pyrochlore to the defect fluorite-type structure with increasing pressure. However, the pressure-induced P-type to F-type structural transition is not complete until a pressure of 28.5 GPa, as evidenced by the weak diffraction peaks from the P-type structure, such as {111} and {133} that are still observed in

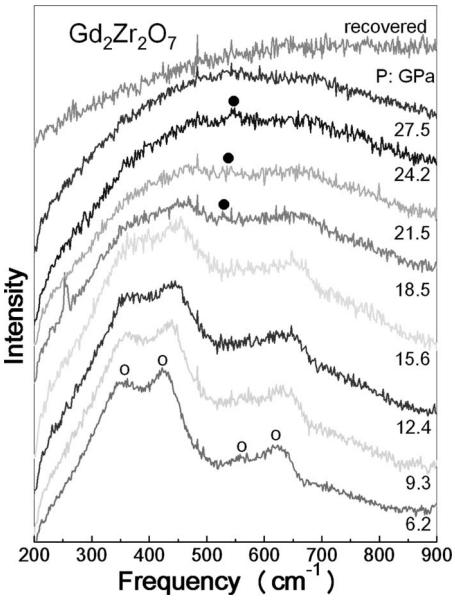

FIG. 3. Raman spectra of $Gd_2Zr_2O_7$ measured at high pressures. The open circles represent the Raman active modes from the pyrochlore structure. A new Raman active mode (marked by ●) appears at 18.5 GPa and is attributed to the high-pressure phase.

the XRD pattern, although the HP phase has already appeared. The transition pressure of the high-pressure phase depends on the different pressure media, it changes from 15.3 GPa with a methonal/ethonal pressure medium to ~23 GPa with argon or nitrogen as the pressure transmitting medium. This may be due to the good hydrostatic pressure condition with Ar and N pressure media. However, the XRD patterns of the HP phase always show a similar character, such as the very broad peak width. In addition, nitrogen and argon pressure transmitting media always produce additional peaks in the XRD patterns due to crystallization, and there are no diffraction peaks from the pressure transmitting medium when methonal/ethonal is used (Fig. 1).

The formation of the HP phase is also confirmed by Raman measurements. The $Gd_2Zr_2O_7$ pyrochlore has at least four observable Raman active modes (open circles) at room conditions. As compared with $Gd_2Ti_2O_7$, these Raman modes are very broad and have low intensities (Fig. 3). The observed Raman spectra have more and more the character of the fluorite structure type[31] with increasing pressure, which indicates the tendency toward the order-disorder transition with increasing pressure. A new Raman mode (solid circle) is observed in the spectrum at 18.5 GPa, which is attributed to the HP phase. Unfortunately, the Raman signal becomes too weak and no Raman active modes can be detected at pressures greater than 30 GPa. The recovered sample is the mixture of the HP phase, defect-fluorite phase, and amorphous based on the XRD measurements, and the Raman spectra (top of Fig. 3) do not provide any useful signals.

The pyrochlore oxides are known to exhibit distortions that result in symmetry changes under certain conditions, such as the formation of tetragonal and monoclinic unit cells.[1] These distorted pyrochlores should have very similar XRD patterns to that of the cubic pyrochlore. The high-pressure phase of $Gd_2Zr_2O_7$ is not a simple structural distortion from the *P*-type structure because of the coexistence of the *P*-type structure and the HP phase and the quite complicated XRD patterns. According to the REE-Zr-O phase diagrams, another phase with composition $A_4B_3O_{12}$ (δ phase) can be formed in a similar compositional region to those systems with small-sized rare-earth elements,[32] such as Dy, Er, and Yb. Experimental results also indicate that there is a volume decrease from the pyrochlore to defect fluorite to the δ phase. Thus, it is reasonable to assume that the HP phase may have a structure similar to that of the δ phase. However, careful study of the XRD patterns and the simulated XRD pattern of the δ phase do not confirm this hypothesis. In fact, the diffraction pattern of the high-pressure phase is quite different from those of pyrochlore, defect fluorite, or the δ phase. The large number of diffraction peaks for the HP phase suggests that high-pressure phase may have a low-symmetry structure. The partial recovery of the fluorite-type structure from the HP phase in the quenched sample indicates that the structure of the HP phase should have a close relation with the *F*-type structure. There is a diffraction peak in the low angle 2θ region of the XRD pattern of the HP phase, which is close to the {111} diffraction peak of the *P*-type structure. The HP phase coexists with pyrochlore structure over a large pressure range (>15 GPa), and the diffraction peaks of the HP phase are quite broad, and the full width at half maximum intensity (FWHM) is generally 2–3 times larger than those of diffraction maxima from the *P*-type structure. This suggests that the formation of the HP phase is very slow, and the disordering of the cations in the HP phase may be not complete, even at high pressures. In the *F*-type structure, the Gd has an equivalent bonding environment as Zr, and the defect *F*-type structure is isotropic with the cubic ZrO_2 except for the absence of 1/8 of the anions. There are two other polymorphs[33] for ZrO_2 besides the high-temperature cubic phase: the monoclinic phase, stable below 1500 K, and the tetragonal phase, stable between 1500–2560 K. Both of these structures can be considered to be distorted fluorite structures. If the Gd and Zr cations in the HP phase have an equivalent bonding environment, the HP phase probably has a structure similar to that of one of the polymorphs of ZrO_2. The HP phase has a diffraction peak in the low angle region, and the structure can only be similar to that of the monoclinic unit cell. We tried to refine the lattice parameters by fitting the XRD patterns with a Rietveld-type calculation, and the lattice parameters and the refined atomic coordinates are listed in Table I. Figure 4 shows the observed XRD pattern at 43.2 GPa together with the calculated XRD pattern and the corresponding diffraction peak positions based on the monoclinic structure model. Though it is difficult to get a satisfactory refinement result (with large *R* factors) for the XRD patterns, the Bragg positions are generally in good agreement with the observed diffraction peaks. The inserted structure (upper right) illustrates the local atomic environment in the HP phase. The cations coordinate with four atoms of O1 and three atoms of O2, and all of these O atoms are at a general position (4*e*). In the HP phase, one of the O1 sites is vacant because of the X_4O_7 stochiometry. Each of the cations, Zr and Gd, are, in fact, coordinated with

TABLE I. The refined atomic coordinates for the high-pressure phase in a monoclinic unit cell (space group: $P2_1/c$) with lattice parameters[a] of $a=5.783$ (9) (Å), $b=3.974$ (7) (Å), $c=4.535$ (6) (Å), and $\beta=99.0°$.

Atom	Wyckoff	x/a	y/b	z/c	Occupancy
Gd (Zr)	4*e*	0.218 (1)	0.031 (2)	0.200 (3)	1
O1	4*e*	0.0705	0.3327	0.3447	0.75
O2	4*e*	0.4499	0.7588	0.4793	1

[a]$R_{\text{Bragg}}=27\%$ and $R_f=15\%$.

six neighboring oxygens. The calculated cell volume of the HP phase is shown in Fig. 5 together with the unit cell volume of the *P*-type $Gd_2Zr_2O_7$. At the upper pressure limit (32 GPa) of the above phase transition, the volume of the HP phase decreases by about 16.4%. For the $Gd_2Zr_2O_7$ pyrochlore, fitting with the Murnaghan equation of state yields to a bulk modulus of Bo=186(12) GPa, when the deviation at zero pressure is fixed at $B'=4$.

Just like the pyrochlore to defect-fluorite phase transition induced by ion irradiation,[12,19,24,27] the formation of the high-pressure phase is also an order-disorder transition process. The cations in the ordered pyrochlore structure swap their positions at high pressures (cation antisite defects), at the same time, anions change their sites from the 8*a* and 48*f* position in pyrochlore structure to the 4*e* positions in the high-pressure phase. At high pressures, the pyrochlore lattice, especially the BO_6 octahedron, is distorted, which may be favorable for the formation of anion Frenkel defects (paired interstitial and vacancy) from the viewpoint of lattice energy.

During the release of pressure, the HP phase is stable at pressures greater than 3.5 GPa. After complete release of

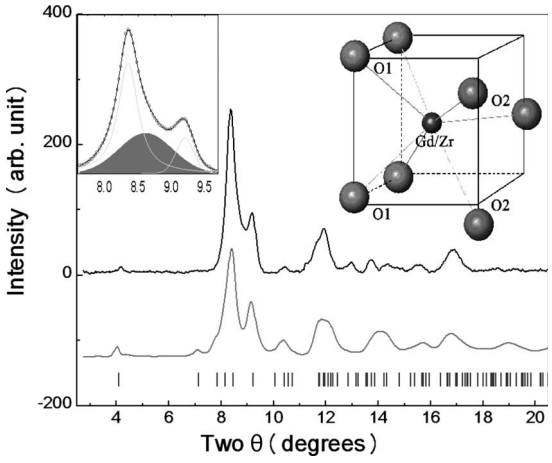

FIG. 4. Calculated and observed XRD profiles (background subtracted) of the HP phase at 43.2 GPa. The vertical bars indicate the position of the ZrO_2-type distorted fluorite structure: monoclinic unit cell, $a=5.78$ Å, $b=3.97$ Å, $c=4.54$ Å, and $\beta=99°$. The upper right inset shows the local atomic structure for the distorted fluorite structure. The square represents the ideal fluorite structure. The left inset shows the peak fitting results at $2\theta=7.6°-9.7°$, and the broad peak reflects the presence of amorphous material.

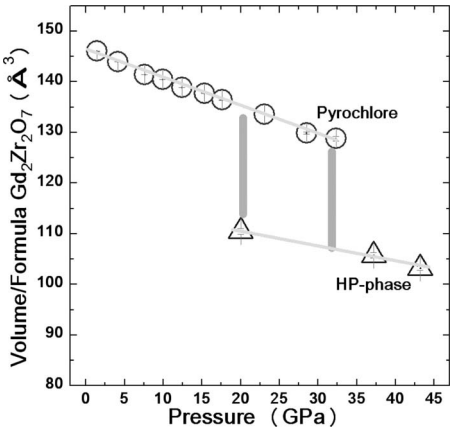

FIG. 5. The calculated unit cell volume per formula unit of $Gd_2Zr_2O_7$ at different pressures. The pyrochlore structure shrinks about 16.4% in volume during phase transition to the high-pressure phase. The two vertical bars mark the pressure regime of two-phase coexistence.

pressure, some sharp diffraction peaks corresponding to the *F*-type structure appear (Fig. 1). This is because the cations are disordered in both the fluorite structure and the HP phase; thus, it is easier for the HP phase to transform to the defect-fluorite structure. In fact, the XRD pattern of the quenched sample is different from the high-pressure phase; that is, there are two broad diffraction peaks between the {222} and {004} diffraction maxima of the pyrochlore structure for the HP phase. The recovered sample only has one broad peak of the HP phase in this region. This indicates that there has probably been another phase transition at lower pressures (e.g., <3.5 GPa) during pressure release. TEM observations have previously confirmed the coexistence of the *F*-type and *P*-type structures in $Cd_2Nb_2O_7$ pyrochlore that was quenched from high pressures,[34] indicating that cation disordering in the HP phase may not have been complete. That may explain why the diffraction peaks of the HP phase of $Gd_2Zr_2O_7$ are so broad.

In addition to the pressure-induced order-disorder transition and the formation of the HP phase, the XRD patterns of the HP phase were always accompanied by a broad shoulder near the strongest diffraction peaks. The peak-fitting result for the XRD pattern at 43.2 GPa in the region near the strongest diffraction peak is shown in the inset (upper left) of Fig. 4. The full width at half maximum (FWHM) of the broad shoulder is about 2–3 times of those of the HP phase and 5–8 times of the *P*-type phase. This suggests the existence of a completely amorphous fraction. Based on the observed XRD patterns, more amorphous phase formed in the quenched sample. Both the HP phase and the amorphous phase from the recovered sample are not stable under ambient conditions and will probably disappear over time. This tendency has been confirmed in another experiment conducted under good hydrostatic conditions. The amount of $Gd_2Zr_2O_7$ with defect-fluorite-type structure increases with time after quenching from a pressure of 44 GPa. The defect-fluorite structure is the most stable phase of $Gd_2Zr_2O_7$, and this is the reason why $Gd_2Zr_2O_7$ is radiation "resistant" and

does not form an amorphous phase, even at very high doses.[21,27]

IV. CONCLUSION

The ordered pyrochlore $Gd_2Zr_2O_7$ has a tendency to transform to the defect-fluorite structure at pressures below 15.3 GPa. A high-pressure phase, which has a distorted defect-fluorite structure, formed through the accumulation of cationic antisite defects at high pressures. Small amounts of amorphous phase were found to coexist with the HP phase. Upon release of pressure, both the HP phase and the amorphous phase are not stable, and they gradually transform to the stable fluorite structure.

ACKNOWLEDGMENTS

This work was supported by the Office of Basic Energy Science of the U.S. Department of Energy, through Grant No. DE-FG02-97ER45656 and the NSF NIRT program (Grant No. EAR-0309772). The use of the National Synchrotron Light Source at the 17C station is supported by NSF COMPRES Contract No. EAR01-35554 and by US-DOE Contract No. DE-AC02-10886.

*rodewing@umuich.edu

[1] M. A. Subramanian, G. Aravamudan, and G. V. Subba Rao, Prog. Solid State Chem. **15**, 55 (1983).
[2] T. Moriga, A. Yoshiasa, F. Kanamaru, K. Koto, M. Yoshimura, and S. Somiya, Solid State Ionics **31**, 319 (1989).
[3] J. Wang, A. Nakamura, and M. Takeda, Solid State Ionics **164**, 185 (2003).
[4] M. P. van Dijk, F. C. Mijlhoff, and A. J. Burggraaf, J. Solid State Chem. **62**, 377 (1986).
[5] A. J. Feighery, J. T. S. Irvine, and C. Zheng, J. Solid State Chem. **160**, 302 (2001).
[6] B. C. Chakoumakos, J. Solid State Chem. **53**, 120 (1984).
[7] S. J. Korf, H. J. A. Koopmans, B. C. Lippens, Jr., A. J. Burggraaf, and P. J. Gellings, J. Chem. Soc., Faraday Trans. 1 **83**, 1485 (1987).
[8] H. Takamura and H. L. Tuller, Solid State Ionics **134**, 67 (2000).
[9] H. Yamamura, H. Nishno, K. Kakimuma, and K. Nomura, Solid State Ionics **158**, 359 (2003).
[10] G. L. Catchen and T. M. Rearick, Phys. Rev. B **52**, 9890 (1995).
[11] K. E. Sickafus, L. Minervini, R. W. Grimes, J. A. Valdez, M. Ishimaru, F. Li, K. J. McClellan, and T. Hartmann, Science **289**, 748 (2000).
[12] B. D. Begg, N. J. Hess, D. E. McCready, S. Thevuthasan, and W. J. Weber, J. Nucl. Mater. **289**, 188 (2001).
[13] L. Minervini and R. W. Grimes, J. Am. Ceram. Soc. **83**, 1873 (2000).
[14] A. F. Reid and A. E. Ringwood, Nature (London) **252**, 681 (1974).
[15] R. D. Shanon and A. W. Sleight, Inorg. Chem. **7**, 1649 (1968).
[16] R. C. Ewing, W. Weber, and J. Lian, J. Appl. Phys. **95**, 5949 (2004).
[17] B. J. Wuensch and K. W. Eberman, JOM **52**, 19 (2000).
[18] C. Heremans, B. J. Wuensch, J. K. Stalick, and E. Prince, J. Solid State Chem. **117**, 108 (1995).
[19] J. Lian, L. M. Wang, J. Chen, K. Sun, R. C. Ewing, J. M. Farmer, and L. A. Boatner, Acta Mater. **51**, 1493 (2003).
[20] P. M. van Dijk, K. J. deVries, and A. J. Burggraaf, Solid State Ionics **9/10**, 913 (1983).
[21] S. X. Wang, B. D. Begg, L. M. Wang, R. C. Ewing, W. J. Weber, and K. V. G. Kutty, J. Mater. Res. **14**, 4470 (1999).
[22] W. J. Weber and R. C. Ewing, Science **5487**, 2051 (2000).
[23] P. Nachimuthu, S. Thevuthasan, V. Shutthnandan, E. M. Adams, W. J. Weber, B. D. Begg, D. K. Shuh, D. W. Lindle, E. M. Gullikson, and R. C. C. Perera, J. Appl. Phys. **97**, 033518 (2005).
[24] J. Lian, X. T. Zu, K. V. G. Kutty, J. Chen, L. M. Wang, and R. C. Ewing, Phys. Rev. B **66**, 054108 (2002).
[25] R. E. Williford and W. J. Weber, J. Nucl. Mater. **299**, 140 (2001).
[26] I. T. Todorov, J. A. Purton, N. L. Allan, and M. T. Dove, J. Phys.: Condens. Matter **18**, 2217 (2006).
[27] J. Lian, L. M. Wang, R. G. Harie, K. B. Helean, and R. C. Ewing, Nucl. Instrum. Methods Phys. Res. B **218**, 236 (2004).
[28] F. X. Zhang, B. Manoun, S. K. Saxena, and C. S. Zha, Appl. Phys. Lett. **86**, 181906 (2005).
[29] F. X. Zhang, B. Manoun, and S. K. Saxena, Mater. Lett. **60**, 2773 (2006).
[30] H. K. Mao, J. Xu, and P. M. Bell, J. Geophys. Res. **91**, 4673 (1986).
[31] N. J. Hess, B. D. Begg, S. D. Conradson, D. E. McCready, P. L. Gassman, and W. J. Weber, J. Phys. Chem. B **106**, 4663 (2002).
[32] K. E. Sickafus, R. W. Grimes, J. A. Valdez, A. Cleave, M. Tang, M. Ishimaru, S. M. Corish, C. R. Stanek, and B. P. Uberuaga, Nat. Mater. **6**, 217 (2007).
[33] M. Yashima, T. Hirose, S. Katano, Y. Suzuki, M. Kakihana, and M. Yoshimura, Phys. Rev. B **51**, 8018 (1995).
[34] F. X. Zhang, J. Lian, U. Becker, R. C. Ewing, L. M. Wang, L. A. Boatner, J. Hu, and S. Saxena, Phys. Rev. B **74**, 174116 (2006).